



## Six-dimensional potential energy surface and rotation–vibration energy levels of HNCO in the ground electronic state

MIRJANA MLADENOVIĆ\*

*Laboratoire Modélisation et Simulation Multi Echelle, MSME UMR8208 CNRS, Université Paris-Est, 5 bd Descartes, 77454 Marne la Vallée, France*

(Received 27 April, revised 8 May, accepted 9 May 2019)

**Abstract:** A six-dimensional potential energy surface based on CCSD(T)/cc-pCVQZ *ab initio* energy points was developed for HNCO in the  ${}^1\text{A}'$  ground electronic state and used to calculate rotation–vibration energy levels for  $J \leq 5$ . The barrier to linearity was computed to be  $1834 \text{ cm}^{-1}$  for the angle HNC and  $336 \text{ cm}^{-1}$  for the angle NCO. The fundamental transitions were obtained for the main form and four isotopic variants of HNCO. The state mixing  $v_3/2v_6$  was identified with the help of an adiabatic projection scheme.

**Keywords:** quasilinear molecules; isotopic variants of HNCO.

### INTRODUCTION

The rovibrational motion of molecules is commonly rationalized applying linear-molecule or bent-molecule formalism. In the bent-linear transition, the rotational degree of freedom of a bent molecule, describing the orbiting about the molecular  $z$ -axis, is transformed into a vibrational degree of freedom of a linear molecule. Isocyanic acid, HNCO, is an example for molecules falling between the two limiting cases of typical linear and typical bent molecules, which are commonly termed quasilinear.<sup>1</sup>

The intriguing vibrational and rovibrational spectroscopy of HNCO, resulting from the molecule's quasilinearity, is of fundamental interest in molecular physics.<sup>1</sup> The infrared spectrum of HNCO was first measured in 1950 by Herzberg and Reid in low resolution.<sup>2</sup> Since then, HNCO has been studied at high spectral resolution in the gas phase in the infrared, far-infrared, microwave, and millimeter wave regions.<sup>3–16</sup> The substitution  $r_s$  structure, derived under the planarity constraint from detailed microwave data of isotopically substituted HNCO, indicated that the molecule has a bent planar structure in a *trans* configuration with an almost linear NCO moiety having a valence angle of  $172^\circ$ .<sup>7,17</sup> The barrier to complete linearity of about  $1900 \text{ cm}^{-1}$  was deduced from a semi-

\* Corresponding author. E-mail: mirjana.mladenovic@u-pem.fr  
<https://doi.org/10.2298/JSC190427039M>

-rigid bender analysis.<sup>18</sup> Under such circumstances, the HNC bending vibration is expected to execute a large amplitude motion at low excitations. In excited bending states, linear arrangements in which strong inter-mode coupling and sizeable coupling to rotation govern the internal dynamics of HNCO were explored. Various kinds of Coriolis interactions were used in effective spectroscopic models for explaining the measured rotation–vibration spectra, complicated by unusually large centrifugal distortion and prominent Coriolis coupling.<sup>5</sup>

In the interstellar medium, HNCO was first detected in 1972 by Snyder and Buhl in Sgr B2.<sup>19</sup> Interstellar deuterated isocyanic acid, DNCO, was identified only recently in an ALMA unbiased spectral survey.<sup>20</sup> HNCO is a constituent of most molecular clouds and a potentially valuable probe of the densest regions.<sup>21</sup> In view of this, isotopic variants of HNCO become interesting for radioastronomy.

Our own interest in isocyanic acid was motivated by a desire to understand the key rotation–vibration spectroscopic features of the molecule from the theoretical point of view. To describe properly the quasilinear behavior of HNCO, an analytical six-dimensional potential energy surface (PES) is required in combination with full-dimensional rotation–vibration calculations involving no dynamical approximations. To the best of our knowledge, only two theoretical studies reported a PES for HNCO. The MP2 study of Pinnavaia *et al.*<sup>22</sup> was, however, in rather poor agreement with experimental results. East *et al.*<sup>23</sup> developed a quartic force field (QFF), refined by adjusting the quadratic force constants to experimentally derived fundamental frequencies, and used the QFF to obtain the spectroscopic properties of HNCO and DNCO by means of the second-order perturbation theory. Serious limitations of QFF representations, as discussed before,<sup>24</sup> prevent their use in combination with variational approaches. A mandatory initial step of the present work was, therefore, the development of a new physically justified PES for HNCO. In the construction of the PES, information previously gathered in detailed studies of structural, spectroscopic, electric, and magnetic properties of the CHNO isomer family, carried out by means of large-scale electronic structure calculations, was relied on.<sup>25–27</sup>

In this work, all rotation–vibration calculations were performed using the atomic masses. In the chemical formulas, the isotope information is provided only when the isotope is not the most abundant.

## RESULTS AND DISCUSSION

### *Potential energy surface*

The six-dimensional potential energy surface for the  ${}^1\text{A}'$  ground electronic state of HNCO was scanned by means of the coupled-cluster CCSD(T) method with full iterative treatment of single and double excitations and a perturbative correction for triple substitutions. Dunning's correlation consistent polarized

core-valence quadruple zeta (cc-pCVQZ) basis set was used, including all electrons in the correlation treatment. All calculations were realized with the Molpro quantum chemistry program package.<sup>28</sup>

The nuclear coordinate space was parameterized in terms of the bond-distance–bond-angle coordinates, described for HNCO by three bond lengths ( $r_1$ ,  $r_2$  and  $r_3$ ), two in-plane bending angles ( $\alpha$  and  $\beta$ ), and one dihedral angle,  $\tau$ , schematically shown in Fig. 1. In total, 948 *ab initio* points were computed.

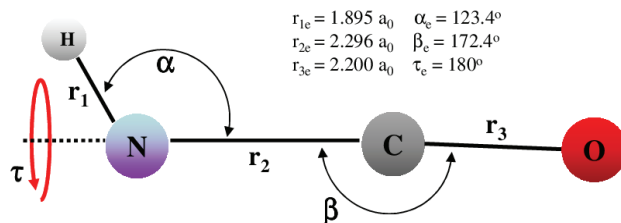


Fig 1. Description of the internal geometry of HNCO in terms of the bond-distance–bond-angle coordinates  $r_1$ ,  $r_2$ ,  $r_3$ ,  $\alpha$ ,  $\beta$ , and  $\tau$ . Their equilibrium values are  $r_{1e}$ ,  $r_{2e}$ ,  $r_{3e}$ ,  $\alpha_e$ ,  $\beta_e$ , and  $\tau_e$ .

#### *Analytical representation of the potential energy surface*

The potential energy *ab initio* data were fitted to the six-dimensional analytical expression of the form:

$$V = V(r_1, r_2, r_3, \alpha, \beta, \tau) = \sum_{ijklmn} C_{ijklmn} s_1^i s_2^j s_3^k P_\ell^n(x_\alpha) P_m^n(x_\beta) \cos(n\tau) \quad (1)$$

The modified Morse coordinates  $s_i$  are used for the radial part, where

$$s_i = 1 - \exp[-a_i(r_i - r_i^{\text{ref}})] \quad (2)$$

for  $i = 1–3$ . The angular part of  $V$  is given by a multipole-like expansion, involving associated Legendre functions  $P_\ell^n(x_\alpha)$  and  $P_m^n(x_\beta)$  with  $\ell, m \geq n$ , where  $x_\alpha = \cos \alpha$  and  $x_\beta = \cos \beta$ .

Optimum values for the six nonlinear parameters  $r_i^{\text{ref}}$  and  $a_i$ , specifying the Morse coordinates  $s_i$  of Eq. (2), were obtained with a Levenberg–Marquardt non-linear least-squares algorithm. For chosen  $r_i^{\text{ref}}$  and  $a_i$ , the expansion parameters  $C_{ijklmn}$  were determined by means of a linear least-squares technique.

For the final fitting, a weight of a  $i^{\text{th}}$  data point of energy  $E_i$  was set to  $1/(E_i + 2000 \text{ cm}^{-1})$ , as previously done.<sup>29</sup> All parameters smaller than one and two times their standard deviation and most of the parameters smaller than three times their standard deviation were eliminated in repeated fitting cycles. In this fashion, a functional six-dimensional expansion consisting of 133 terms was obtained. The standard deviation of the weighted 133-term representation was  $3.2 \text{ cm}^{-1}$ . The expansion coefficients  $C_{ijklmn}$  are summarized in Table I. The zero of the energy scale is defined as the energy of the minimum, obtained at  $-168.658308 E_h$  in electronic structure computations.

TABLE I. Expansion coefficients  $C_{ijklmn}$  (in atomic units) of Eq. (1) for the six-dimensional CCSD(T)/cc-pCVQZ PES derived in this work for the ground electronic state of HNCO; the reference distances  $r_1^{\text{ref}} = 2.71421a_0$ ,  $r_2^{\text{ref}} = 2.182717a_0$ ,  $r_3^{\text{ref}} = 2.306116a_0$ , and the exponential parameters  $a_1 = 1.802784a_0^{-1}$ ,  $a_2 = 0.16607a_0^{-1}$ ,  $a_3 = 1.783286a_0^{-1}$  specify the Morse coordinates  $s_i$  defined by Eq. (2)

$ijklmn$	$C_{ijklmn}$	$ijklmn$	$C_{ijklmn}$	$ijklmn$	$C_{ijklmn}$
200000	0.53734802	000111	0.15655068	010100	0.92563963
300000	-0.11484194	000211	0.07935772	010110	2.02033491
400000	0.55012451	000311	0.01233358	010120	1.29061412
500000	0.50933854	000411	0.00522150	010130	0.29939787
020000	3.04343472	000511	0.00137902	010200	0.00519847
030000	-6.42701702	000121	0.10338936	010210	-0.07831394
040000	6.26800904	000221	0.06221133	010111	0.02006594
002000	1.95205229	000321	0.00394642	010211	-0.01992492
003000	-2.25595405	000421	0.00173606	010311	0.00947693
004000	-0.24432277	000521	0.00044231	010222	0.00318433
011000	1.69434111	000131	0.03952968	011010	1.68516058
012000	-0.09925057	000231	0.02399362	011020	0.35846689
021000	-0.06589205	000141	0.00688751	011100	0.00158883
101000	0.19172852	000241	0.00425318	011111	-0.03904475
102000	-0.04106384	000222	0.00100867	020100	0.07663680
110000	0.21018867	000322	0.00067019	020200	0.06593700
111000	0.07486716	000422	0.00030567	020211	-0.03995808
120000	-0.13855202	000522	0.00003161	021100	0.42999220
000100	0.56031380	000232	0.00019589	030111	-0.46136386
000200	0.85158071	000332	0.00007405	100010	-0.26294530
000300	0.22700620	000432	0.00003174	100020	-0.16673037
000400	0.47937879	000242	0.00002612	100030	-0.04143013
000500	0.25138665	000333	0.00001639	100100	-0.16217242
000600	0.10114673	000433	-0.00000006	100110	0.01171819
000700	0.02938479	000343	0.00000174	100200	-0.06319147
000800	0.00444831	001010	0.08434281	100300	-0.01713216
000010	-0.98939957	001020	0.38507953	100111	0.02035922
000110	-0.06125517	001030	0.12828422	100121	-0.00656677
000210	0.43724286	001100	0.74606740	100221	-0.00693010
000310	-0.80352398	001110	1.43891290	100311	0.00615047
000410	0.05517163	001120	0.90447861	100222	0.00033481
000510	0.01340130	001130	0.21616529	101010	0.23017684
000020	-1.30718639	001200	-0.07611864	101100	0.25027328
000120	-0.05905497	001210	-0.04684352	101110	0.24034936
000220	0.63105974	001111	-0.05802572	101111	-0.04933778
000320	-0.56603202	001121	-0.00815440	102111	-0.31868518
000030	-0.85192952	001211	0.00339054	110100	0.39396562
000130	-0.07394863	001311	-0.00527136	110200	0.15795861
000230	0.52080080	002100	0.20979836	110111	-0.07852199
000330	-0.13053770	002110	0.21799448	110211	-0.02597514
000040	-0.35275207	002111	-0.10678379	200100	0.03824237

TABLE I. Continued

$ijklmn$	$C_{ijklmn}$	$ijklmn$	$C_{ijklmn}$	$ijklmn$	$C_{ijklmn}$
000140	-0.14394497	010010	0.94117031	200200	0.04047474
000240	0.15153858	010020	0.88024957	200111	0.00699700
000050	-0.07464887	010030	0.23321474	300010	0.04798472
000150	-0.06495179				

For the CCSD(T)/cc-pCVQZ PES, the structural parameters [ $r_{1e}$ ,  $r_{2e}$ ,  $r_{3e}$ ,  $\alpha_e$ ,  $\beta_e$ ] of the optimum planar configuration are [1.8953 $a_0$ , 2.2958 $a_0$ , 2.2000 $a_0$ , 123.37°, 172.45°], see also Fig. 1. The agreement with the experimental structure derived by East *et al.*<sup>23</sup> as [1.8960 $a_0$ , 2.2960 $a_0$ , 2.1991 $a_0$ , 123.29°, 172.37°] is within 0.0009 $a_0$  for the bond lengths and 0.08° for the bond angles. The equilibrium rotational constants  $A_e$ ,  $B_e$  and  $C_e$  are 28.05, 0.370 and 0.365 cm<sup>-1</sup> for HNCO and 16.05, 0.345 and 0.338 cm<sup>-1</sup> for DNCO. Isocyanic acid is a nearly prolate symmetric top, with a value  $\kappa = -0.9997$  for the Ray asymmetry parameter. The harmonic frequencies calculated for the present PES are 3712, 2317, 1317, 803, 565 and 635 cm<sup>-1</sup> for HNCO and 2737, 2293, 1298, 731, 459 and 622 cm<sup>-1</sup> for DNCO.

#### Topography of the potential energy surface

The two-dimensional maps of the six-dimensional CCSD(T)/cc-pCVQZ PES are displayed in Fig. 2.

The maps in Fig. 2 were computed by freezing the remaining four coordinates at their equilibrium values. The contour plots ( $\tau, \alpha$ ) and ( $\tau, \beta$ ) involving the dihedral angle  $\tau$  clearly show that HNCO is a planar molecule possessing only a *trans* minimum. The most prominent coupling seen in Fig. 2 is between the HNC bending angle  $\alpha$  and the NC bond length  $r_2$ . Fig. 2 also displays the variation of the internal coordinate on the  $y$ -axis along the minimum energy path (MEP) in the direction of the coordinate shown on the  $x$ -axis (red lines). The MEP along  $\tau$  was computed by minimizing  $V$  with respect to the remaining five coordinates, whereas the MEPs for  $\alpha$  and  $\beta$  were determined for the planar arrangement with  $\tau = 180^\circ$ .

The variations of the potential energy along the MEPs in the direction of the angles  $\alpha$ ,  $\beta$ , and  $\tau$  are depicted in Fig. 3. The barrier to linearity for the in-plane bending angles HNC and NCO is 1834 and 336 cm<sup>-1</sup> along the respective MEP. The MEPs are compared with the one-dimensional cut,  $V^{\text{cut}}$ , obtained by freezing all other coordinates at their equilibrium values. The value of  $V^{\text{cut}}$  at  $\alpha = 180^\circ$  is 968 cm<sup>-1</sup> larger than the corresponding MEP value, whereas  $V^{\text{cut}}$  and  $V^{\text{MEP}}$  for  $\tau = 0^\circ$  differ even by 1017 cm<sup>-1</sup>. In view of this, it is reasonable to expect an important role of both the in-plane angle  $\alpha$  and the torsional angle  $\tau$  in the internal dynamics of HNCO.

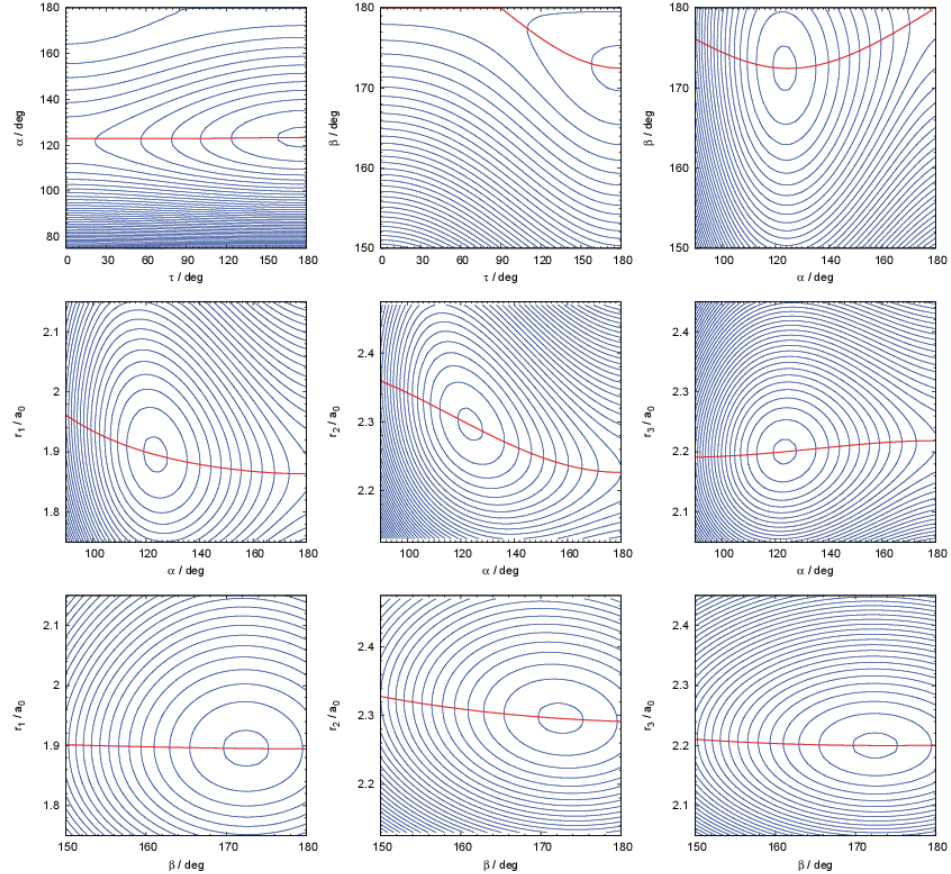


Fig. 2. Two-dimensional contour maps of the CCSD(T)/cc-pCVQZ PES, obtained with the remaining four coordinates kept constant at their equilibrium values. Contour lines are drawn in intervals of  $250 \text{ cm}^{-1}$  with the first contour placed at  $50 \text{ cm}^{-1}$ . The solid (red) line shows the variation of the coordinate on the y-axis along the minimum energy path in the direction of the coordinate on the x-axis.

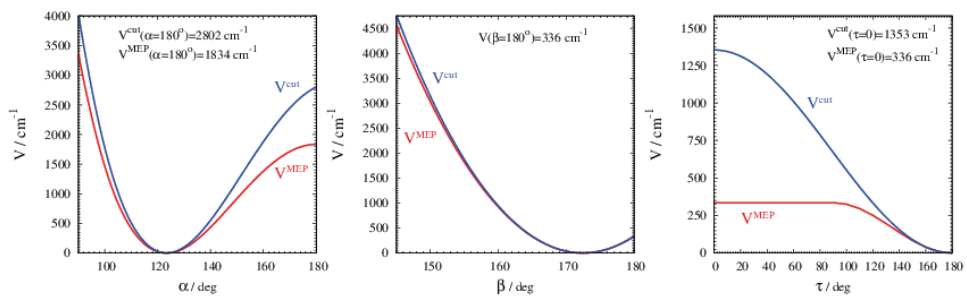


Fig. 3. Minimum energy path  $V^{\text{MEP}}$  and the one-dimensional cut  $V^{\text{cut}}$  along the HNC angle  $\alpha$ , the NCO angle  $\beta$ , and the torsion angle  $\tau$ .

The optimum triple ( $r_1$ ,  $r_2$ ,  $r_3$ ) along the  $\alpha$  MEP changes from ( $1.895a_0$ ,  $2.296a_0$ ,  $2.200a_0$ ) for  $\alpha = \alpha_e = 123.4^\circ$  into ( $1.863a_0$ ,  $2.226a_0$ ,  $2.219a_0$ ) for  $\alpha = 180^\circ$ , such that the straightening of the HNC bending angle decreases  $r_1(\text{HN})$  and  $r_2(\text{NC})$  by  $0.032$  and  $0.070a_0$ , respectively, while  $r_3(\text{CO})$  increases by  $0.019a_0$ . The torsional MEP assumes a constant value of  $336 \text{ cm}^{-1}$  for  $\tau \leq 90^\circ$ . The optimum “hockey-stick” structure for a strictly linear heavy atom NCO skeleton is given by ( $1.895a_0$ ,  $2.291a_0$ ,  $2.201a_0$ ) and  $\alpha = 122.9^\circ$ . This configuration is only marginally changed relative to the equilibrium.

#### Rovibrational state calculations

The rovibrational calculations were realized by means of the DVR(+R)+FBR approach, which is designed for the body-fixed formulation of the kinetic energy operator.<sup>29–32</sup> The orthogonal (diatom+diatom) coordinates ( $d_1$ ,  $d_2$ ,  $R$ ,  $\theta_1$ ,  $\theta_2$ ,  $\chi$ ), schematically shown in Fig. 4, were used.<sup>30</sup> The coordinates  $d_1$  and  $d_2$  refer to the HN and CO bond lengths,  $R$  is the distance between the centers of mass of the HN and CO subunits,  $\theta_i$  is the angle enclosed by the vectors  $\mathbf{d}_i$  and  $\mathbf{R}$ , and  $\chi$  is the out-of-plane (torsional) angle. The body-fixed  $z$ -axis is placed along the vector  $\mathbf{R}$ .

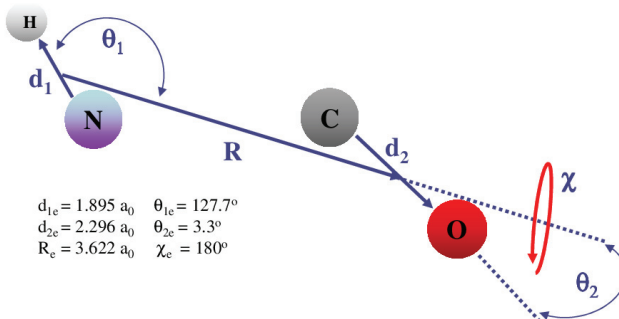


Fig. 4. Orthogonal (diatom+diatom) internal coordinates  $d_1$ ,  $d_2$ ,  $R$ ,  $\theta_1$ ,  $\theta_2$  and  $\chi$  used in the rovibrational calculations.

The DVR(+R)+FBR approach employs the parity-adapted rotation-angular basis, specified with total rotational angular momentum  $J$  and parity  $p$  as strictly conserved quantum numbers. The permitted values of the quantum number  $K$  of the  $z$ -projection of  $\mathbf{J}$  are  $K \in [0, J]$  in the parity-adapted formulation. The quantum number  $k$  of the body-fixed projection of the vibrational angular momentum is related to the torsional primary space. The computational strategy uses combined discrete variable and finite basis representations for the angular coordinates ( $\theta_1$ ,  $\theta_2$ ,  $\chi$ ) in combination with a discrete Jacobi distance  $R$ , eigenfunctions for ( $d_1, d_2$ ), and symmetric top eigenfunctions for the rotational part.<sup>31</sup> The sequen-

tial inclusion of the internal degrees of freedom together with contraction schemes resulting from several diagonalization and truncation steps allows the construction of a final full-dimensional Hamiltonian matrix of relatively modest size.<sup>32</sup> Matrix diagonalizations were performed by conventional dense matrix algorithms to give eigenenergies and eigenfunctions.

The computed rovibrational states were characterized with the help of the adiabatic projection method, which employs zero-order basis functions constructed in the adiabatic  $R$ -stretch approximation following the quantum-state character correlation scheme.<sup>32</sup> The stretching states  $|\alpha\rangle$ , adiabatically separated from the remaining five vibrational modes, were calculated for the  $i^{\text{th}}$  five-mode state, yielding the zero-order (adiabatic) vectors  $|\alpha, i; K\rangle$  for a given  $K$ . The adiabatic vectors  $|\alpha, i; K\rangle$  were used to calculate the adiabatic expansions of numerically exact wavefunctions  $|n; J\rangle$  for a given  $J$  as:

$$|n; J\rangle = \sum C_{\alpha, i, K} |\alpha, i; K\rangle \quad (3)$$

This expansion supplies a zero-order origin of the state  $|n; J\rangle$  by locating the dominant adiabatic contribution among all  $|\alpha, i; K\rangle$ .

The rovibrational calculations were performed for  $J=0-5$  in both parities. In the actual computations, the pointwise representation for the Jacobi distance  $R$  included 12 unevenly distributed potential optimized discrete points. The eigenfunction set  $(n_{d1}, n_{d2}) = (3,6)$  was used for the coordinates  $(d_1, d_2)$ . The maximum value of the projection quantum number  $k$  was 8 for  $J=0$  and 13 for  $J=5$ . The integrals over the dihedral angle were solved by means of the Gauss–Chebyshev quadrature of order 15, whereby  $\chi \in (0^\circ, 180^\circ)$ . Truncated sets of Gauss–Legendre discrete points were used for the bending angles, keeping only the points  $\theta_1 \in (70^\circ, 180^\circ)$  together with  $\theta_2 \in (0^\circ, 50^\circ)$ . The resulting primary basis included approximately 900,000 functions for  $J=0$  and 10,000,000 functions for  $J=5$ . The truncation of the primary basis set was made with several cutoff parameters, which are employed at different stages of the calculation. For a given  $K$  and  $J$ , the size of the vibrational six-dimensional matrix was 8400. The size of the final nine-dimensional rotation–vibration Hamiltonian matrix was 800 and 2400 for  $J=1$  and  $5$ , respectively. The calculations took about 8 and 150 CPU h for, respectively,  $J=0$  and  $J=5$  (single parity) on a single processor (Intel Xeon). The CPU times refer to the calculation of eigenenergies with eigenvectors and to the eigenfunction analysis for a large number of calculated states (up to 700).

#### Fundamental transitions

The fundamental transitions calculated using the present CCSD(T)/cc-pCVQZ PES for HNCO, DNCO, H<sup>15</sup>NCO, HN<sup>13</sup>CO, and HNC<sup>18</sup>O are summarized in Table II. The state assignments were made in terms of v<sub>1</sub>, v<sub>2</sub>, v<sub>3</sub>, v<sub>4</sub>, v<sub>5</sub>, v<sub>6</sub> following the nonlinear-molecule model. The mode labels v<sub>1</sub>, v<sub>2</sub>, v<sub>3</sub> refer to the

HN stretch, the antisymmetric NCO stretch, and the symmetric NCO stretch, respectively. The labels  $v_4$  and  $v_5$  describe the in-plane bending modes, and  $v_6$  is the out-of-plane bending mode (the torsion). The torsional transitions were determined from the odd-parity  $J=0$  computation since the out-of-plane bending mode  $v_6$  belongs to the  $A''$  irreducible representation of the  $C_s$  symmetry group, as seen in Table II.

TABLE II. Fundamental wavenumbers and zero-point energy  $E_0$ , with high-resolution gas-phase spectroscopic data shown in square brackets; all quantities in  $\text{cm}^{-1}$

Mode	HNCO	DNCO	$\text{H}^{15}\text{NCO}$	$\text{HN}^{13}\text{CO}$	$\text{HNC}^{18}\text{O}$
$v_1 (a')$	3550.0 [3538.3] <sup>a,b</sup>	2643.5 [2638.8] <sup>h</sup>	3540.3	3550.1	3547.6
$v_2 (a')$	2276.9 [2268.9] <sup>c,d</sup>	2249.6	2269.0	2216.4	2256.9
$v_3 (a')$	1323.8 [1322.3] <sup>e</sup>	1306.4	1248.4	1316.0	1241.8
$v_4 (a')$	778.4 [776.6] <sup>f</sup>	725.0	772.9	767.1	776.5
$v_5 (a')$	574.4 [577.4] <sup>f</sup>	455.9	573.8	567.4	571.1
$v_6 (a'')$	658.5 [656.3] <sup>g</sup>	633.2	656.5	641.5	653.3
$E_0$	4625.8	4038.3	4602.9	4575.6	4592.9

<sup>a</sup>Ref. 12; <sup>b</sup>ref. 15; <sup>c</sup>ref. 9; <sup>d</sup>ref. 10; <sup>e</sup>ref. 16; <sup>f</sup>ref. 6; <sup>g</sup>ref. 11; <sup>h</sup>ref. 8

The results for  $v_1$  in Table II agree with known experimental data within  $12 \text{ cm}^{-1}$  for HNCO and  $5 \text{ cm}^{-1}$  for DNCO. For HNCO, the agreement is within  $8 \text{ cm}^{-1}$  for  $v_2$  and within  $3 \text{ cm}^{-1}$  for  $v_3-v_6$ . For DNCO, Ashby and Werner<sup>3</sup> observed  $v_1 = 2634.9 \text{ cm}^{-1}$ ,  $v_2 = 2235 \text{ cm}^{-1}$ , and  $v_3 = 1310 \text{ cm}^{-1}$  under low spectral resolution. The theoretical predictions for ( $v_1, v_2, v_3, v_4, v_5, v_6$ ) by East *et al.*<sup>23</sup> are given as (2642, 2236, 1307, 727, 458, 633) for DNCO, with the values in parentheses given in  $\text{cm}^{-1}$ . The matrix isolation fundamental transitions  $v_4 = 722.4$  (721.4)  $\text{cm}^{-1}$  and  $v_5 = 460.1$  (458.1)  $\text{cm}^{-1}$  were reported by Bondybey *et al.*<sup>33</sup> for DNCO in solid Ar (Ne).

Hitherto, no gas-phase vibrational transitions have been reported for the rare isotopologues of HNCO. Teles *et al.*<sup>34</sup> measured infrared spectra of  $\text{H}^{15}\text{NCO}$  and  $\text{HN}^{13}\text{CO}$  in solid Ar at 13 K, reporting  $v_1 = 3502.6 \text{ cm}^{-1}$ ,  $v_2 = 2250.8 \text{ cm}^{-1}$ ,  $v_4 = 764.4 \text{ cm}^{-1}$ , and  $v_5 = 573.0 \text{ cm}^{-1}$  for  $\text{H}^{15}\text{NCO}$  and  $v_1 = 3514.9 \text{ cm}^{-1}$ ,  $v_2 = 2199.0 \text{ cm}^{-1}$ ,  $v_4 = 758.8 \text{ cm}^{-1}$ , and  $v_5 = 566.3 \text{ cm}^{-1}$  for  $\text{HN}^{13}\text{CO}$ .

#### Rotational K excitations

The goodness of the quantum number  $K$  of the  $z$ -projection of the overall angular momentum  $J$  was investigated by evaluating the probabilities  $(J)P_K$  that the wavefunction takes for a certain  $K$  value. For HNCO, the quantum label  $K$  is found to be essentially a good quantum number, with  $(J)P_K \geq 0.98$ . For a given vibrational state, the energies of the  $K$  sublevels are well separated owing to the large rotational  $A$  constant. This is seen in Fig. 5, showing the rotational excitation in the lowest vibrational states for  $J=0-5$ .

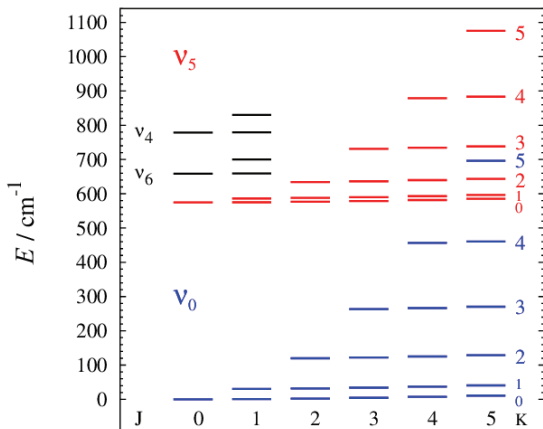


Fig. 5. Rotational excitation in the ground vibrational state  $\nu_0$  and in the  $\nu_5$  state of HNCO for  $J = 0-5$ . For  $\nu_4$  and  $\nu_6$ , only the levels with  $J = 0, 1$  are depicted.

The rotational levels with  $K \neq 0$  are doubly degenerate in Fig. 5. The energy levels exhibit a relatively large asymmetry splitting only for  $K = 1$ . For instance, the energy difference between the ground-state levels of odd and even parity is  $0.0054 \text{ cm}^{-1}$  for  $K = 1$  and in the order of  $10^{-6}$ ,  $10^{-9}$  and  $10^{-11} \text{ cm}^{-1}$  for  $K = 2, 3$ , and  $4$ , respectively. The  $K = 1$  levels of  $\nu_0$ ,  $\nu_4$ ,  $\nu_5$ ,  $\nu_6$  lie  $29.9$ ,  $11.2$ ,  $40.8$ ,  $51.1 \text{ cm}^{-1}$ , respectively, above the respective  $K = 0$  state. A comparison with the experimental values of Niedenhoff and coworkers,<sup>13</sup> which are given by  $30.1$ ,  $9.2$ ,  $43.4$  and  $51.3 \text{ cm}^{-1}$ , shows agreement within  $2.6 \text{ cm}^{-1}$ .

The rotational energy level separation  $\Delta_b(J, K \rightarrow J', K')$  for a given vibrational state  $\nu_b$  is computed as:

$$\Delta_b(J, K \rightarrow J', K') = E_b(J', K') - E_b(J, K) \quad (4)$$

When  $J' = J$  and  $K' = K+1$ , then  $\Delta_b(J, K \rightarrow J, K+1)$  provides the energy for the rotational  $Q$ -branch transition  ${}^RQ_K(J)$ , where the usual notation  ${}^{\Delta K}\Delta_{JK}$  is used. For the ground vibrational state  $\nu_b = \nu_0$  of HNCO, the values of  $\Delta_0(J, K \rightarrow J, K+1)$  were determined to be  $29.90$ ,  $87.73$ ,  $141.37$ ,  $190.45$  and  $239.20 \text{ cm}^{-1}$  for  $K = 0$ ,  $1$ ,  $2$ ,  $3$ , and  $4$ , respectively, using  $J = K+1$ . The corresponding experimental values for  ${}^RQ_K$  were reported by Krakow *et al.*<sup>4</sup> as  $30.04$ ,  $88.26$ ,  $142.20$ ,  $191.78$ , and  $237.04 \text{ cm}^{-1}$ . Thus, the present results agree with the experimental finding within  $2.2 \text{ cm}^{-1}$ , *i.e.* within 1 %.

For the transitions  $\nu_{0,K} \rightarrow \nu_{b,K'}$  from the ground vibrational state  $\nu_0$  with  $K$  to the vibrational state  $\nu_b$  with  $K'$ , the transition energy  $\Delta_{b,0}(J, K \rightarrow J', K')$  was calculated as:

$$\Delta_{b,0}(J, K \rightarrow J', K') = E_b(J', K') - E_0(J, K) \quad (5)$$

The values for  $\Delta_{b,0}(J,K \rightarrow J',K')$  obtained using  $J' = K'$  and  $J = K$  are compared in Table III with the experimental sub-band centers reported by Steiner *et al.*<sup>6</sup> for the singly excited states of  $v_4$ ,  $v_5$  and  $v_6$ . The results in Table III agree with the experimentally derived values within  $3\text{ cm}^{-1}$  in the case of  $v_4$  and  $v_5$ , whereas deviations of up to  $8.2\text{ cm}^{-1}$  are seen for  $v_6$ .

TABLE III. Transition energies (in  $\text{cm}^{-1}$ ) for  $v_0, K \rightarrow v_b, K'$  and  $v_b = v_4, v_5, v_6$ ; experimental values shown in square brackets are taken from Ref. 6

$K'$	$K$	$v_5$	$v_6$	$v_4$
0	0	574.4 [577.4]		778.4 [776.6]
1	1	555.8 [556.5]	669.4 [669.6]	799.7 [797.9]
2	2	514.4 [512.9]	696.1 [698.9]	842.4 [840.8]
3	3	467.7 [465.2]	728.8 [733.0]	890.1 [888.8]
4	4	422.3	762.5 [767.4]	937.6 [936.4]
5	5	379.6	793.6 [801.8]	982.8 [981.7]
0	1	543.8	627.9	747.8 [746.5]
1	2	466.6	580.2	710.5 [709.6]
2	3	370.8	552.5	698.8 [698.5]
1	0	586.4	700.0	830.2 [828.0]
2	1	603.6	785.3	931.6 [929.0]
3	2	611.3	872.4	1033.7 [1031.0]

The transition  $Q_0 Q_0$  for  $v_6$  was not observed in Ref. 6. Fusina *et al.*<sup>11</sup> found  $Q_0 Q_0$  at  $43.44\text{ cm}^{-1}$  and deduced  $v_6 = 656.287\text{ cm}^{-1}$  from the energy of  $699.731\text{ cm}^{-1}$  for the level  $v_6 = 1$  and  $K = 1$  derived by Yamada.<sup>35</sup> Niedenhoff *et al.*<sup>14</sup> obtained the  $K$  rotational levels of  $v_6$  as  $656.3$ ,  $699.7$ ,  $817.3$ ,  $993.6$ ,  $1219.7$ ,  $1491.0\text{ cm}^{-1}$  for  $K = 0 - 5$  from a Padé-type fit, which included Coriolis interaction between the three bending states. The present results for  $v_6 = 1$  are respectively  $658.5$ ,  $700.0$ ,  $815.9$ ,  $992.2$ ,  $1219.4$  and  $1489.6\text{ cm}^{-1}$  for  $K = 0 - 5$ , showing an agreement within  $2.2\text{ cm}^{-1}$  with the prediction from Ref. 14.

### The stretching $v_3$ fundamental

The fundamental  $v_3$  wavenumber in Table II is  $1323.8\text{ cm}^{-1}$ . This result is in good agreement with the experimental value  $v_3 = 1327\text{ cm}^{-1}$  obtained by Herzberg and Reid<sup>2</sup> from gas-phase infrared spectra and  $v_3 = 1322\text{ cm}^{-1}$  obtained by Brown *et al.*<sup>16</sup> from photoacoustic Raman spectra.

The calculated rotation–vibration energy levels were characterized with the help of the adiabatic projection method. This analysis led to the identification of  $v_3/2v_6$  mixing. For the states  $2v_6$  and  $v_3$  of HNCO, the adiabatic expansions of Eq. (3) expressed in terms of the zero-order vectors  $| \alpha, i; K \rangle$  read:

$$| 2v_6 \rangle = 0.696 | 0,4;0 \rangle - 0.604 | 1,0;0 \rangle \quad (6)$$

$$| v_3 \rangle = 0.623 | 0,4;0 \rangle + 0.657 | 1,0;0 \rangle \quad (7)$$

where level  $2v_6$  occurs at  $1260.8\text{ cm}^{-1}$ . The notation used by the code for  $|\alpha, i; K\rangle$  was employed in Eqs. (6) and (7), with  $|0,4;0\rangle$  and  $|1,0;0\rangle$  denoting the adiabatic  $2v_6$  and  $v_3$  states with  $K = 0$ , respectively. The two-component expansions of Eqs. (6) and (7) provide more than 80 % of the respective full-dimensional wavefunctions. The adiabatic states  $|1,0;0\rangle$  and  $|0,4;0\rangle$  contribute with respectively 43 and 39 % to  $|v_3\rangle$  and with 36 and 48 % to  $|2v_6\rangle$ . The  $v_3/2v_6$  mixing was found in all isotopic variants of HNCO studied herein.

For the low-lying vibrational states of HNCO, the full-dimensional energies  $E^{(J,p)}$  computed for  $J=0$  and both parities ( $p=0$  and  $p=1$ ) are compared in Fig. 6 with energies  $\epsilon_R^{(J,p)}$  obtained using a single discrete point  $R = 3.608a_0$ . The levels  $E^{(0,p)}$ , obtained upon inclusion of the coordinate  $R$ , are above  $\epsilon_R^{(0,p)}$  for all the states shown in Fig. 6, except for  $2v_6$ . In the case of  $2v_6$ , the level  $E^{(0,0)}$  at  $1261\text{ cm}^{-1}$  is  $11\text{ cm}^{-1}$  below  $\epsilon_R^{(0,0)}$  at  $1272\text{ cm}^{-1}$ . Due to the mixing of the zero-order states  $|0,4;0\rangle$  and  $|1,0;0\rangle$ , the upper of the two levels is pushed higher up in energy. This provides the key line of argument for assigning  $v_3$  to the state at  $1324\text{ cm}^{-1}$  in Table II.

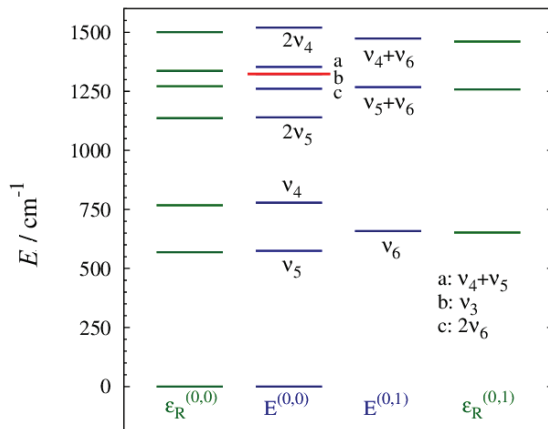


Fig. 6. Full-dimensional energies  $E^{(J,p)}$  and energies  $\epsilon_R^{(J,p)}$  calculated using a single R DVR point.

The level  $v_5 + v_6$  at  $1268\text{ cm}^{-1}$  is seen between  $2v_6$  and  $v_3$  in Fig. 6. For reasons of symmetry,  $v_5 + v_6$  does not interact with  $2v_6$  and  $v_3$  for  $J=0$ . In rotationally excited HNCO with  $J \neq 0$ , three levels are found to interact via Coriolis coupling. More details on these results will be discussed elsewhere, along with the results regarding the rotational behavior of the stretching  $v_1$  and  $v_2$  vibrations.

## CONCLUSIONS

This work presents quantum mechanical calculations for HNCO performed with the DVR(+R)+FBR method using a new *ab initio* CCSD(T)-cc-pCVQZ pot-

ential energy surface. The rovibrational energy levels were computed and analyzed for total rotational angular momentum  $J \leq 5$  in both parities. Resonance interaction of the  $v_3$  stretching mode with  $2v_6$  occurs in all five isotopic variants of HNCO studied herein.

The potential energy surface developed in this work captures the main quasi-linear features of the HNCO molecule. Since the barrier to complete linearity can be overcome with moderate vibrational energies in HNCO, it is now important to examine how the level pattern changes with energy. Recognition of different energy level patterns in different energy regions, such as in isomerizing linear triatomic molecules,<sup>36</sup> is important for understanding the details of the underlying physics. Work along these lines is proceeding.

*Acknowledgements.* The author would like to express her gratitude to Professor Miljenko Perić for the patient guidance, encouragement, and inspiring discussions during her Ph.D. thesis at the University of Belgrade, which left an unforgettable mark and laid the foundation for her future work.

#### ИЗВОД

#### ШЕСТОДИМЕНЗИОНАЛНА ПОВРШ ПОТЕНЦИЈАЛНЕ ЕНЕРГИЈЕ И РОТАЦИОНО- -ВИБРАЦИОНА СТАЊА МОЛЕКУЛА ННКО У ОСНОВНОМ ЕЛЕКТРОНСКОМ СТАЊУ

МИРЈАНА МЛАДЕНОВИЋ

*Laboratoire Modélisation et Simulation Multi Echelle, MSME UMR8208 CNRS, Université Paris-Est, 5 bd Descartes, 77454 Marne la Vallée, France*

Шестодимензионална површ потенцијалне енергије за HNCO у основном електронском стању је конструисана на бази *ab initio* тачака електронске енергије квалитета CCSD(T)/cc-pCVQZ и примењена у прорачуну ротационо-вибрацијских енергетских нивоа за  $J \leq 5$ . Баријера према линеарном аранжману износи  $1834 \text{ cm}^{-1}$  у правцу угла HNC и  $336 \text{ cm}^{-1}$  у правцу угла NCO. Фреквенције основних прелаза су дате за главни облик и четири изомеријске варијанте молекула HNCO. Користећи метод адијабатских пројекција утврђено је мешање типа  $v_3/2v_6$ .

(Примљено 27. априла, ревидирано 8. маја, прихваћено 9. маја 2019)

#### REFERENCES

1. B. P. Winnewisser, in *Molecular Spectroscopy: Modern Research*, Vol. 3, K. Narahari Rao, Ed., Academic Press, Orlando, FL, 1985, p 321 (<https://doi.org/10.1016/B978-0-12-580643-5.50011-7>)
2. G. Herzberg, C. Reid, *Discuss. Faraday Soc.* **9** (1950) 92 (<https://doi.org/10.1039/DF9500900092>)
3. R. A. Ashby, R. L. Werner, *Spectrochim. Acta* **22** (1966) 1345 ([https://doi.org/10.1016/0371-1951\(66\)80038-3](https://doi.org/10.1016/0371-1951(66)80038-3))
4. B. Krakow, R. C. Lord, G. O. Neely, *J. Mol. Spectrosc.* **27** (1968) 148 ([https://doi.org/10.1016/0022-2852\(68\)90027-1](https://doi.org/10.1016/0022-2852(68)90027-1))
5. K. M. T. Yamada, *J. Mol. Spectrosc.* **68** (1977) 423 ([https://doi.org/10.1016/0022-2852\(77\)90246-6](https://doi.org/10.1016/0022-2852(77)90246-6))
6. D. A. Steiner, K. A. Wishah, S. R. Polo, T. K. McCubbin, Jr., *J. Mol. Spectrosc.* **76** (1979) 341 ([https://doi.org/10.1016/0022-2852\(79\)90233-9](https://doi.org/10.1016/0022-2852(79)90233-9))

7. K. M. T. Yamada, *J. Mol. Spectrosc.* **79** (1980) 323 ([https://doi.org/10.1016/0022-2852\(80\)90217-9](https://doi.org/10.1016/0022-2852(80)90217-9))
8. D. A. Steiner, S. R. Polo, T. K. McCubbin, K. A. Wishah, *Can. J. Phys.* **59** (1981) 1313 (<https://doi.org/10.1139/p81-172>)
9. B. Lemoine, K. Yamada, G. Winnewisser, *Ber. Bunsenges. Phys. Chem.* **86** (1982) 795 (<https://doi.org/10.1002/bbpc.19820860906>)
10. D. A. Steiner, S. R. Polo, T. K. McCubbin, Jr., K. A. Wishah, *J. Mol. Spectrosc.* **98** (1983) 453 ([https://doi.org/10.1016/0022-2852\(83\)90254-0](https://doi.org/10.1016/0022-2852(83)90254-0))
11. L. Fusina, M. Carlotti, B. Carli, *Can. J. Phys.* **62** (1984) 1452 (<https://doi.org/10.1139/p84-192>)
12. K. M. T. Yamada, M. Winnewisser, J. W. C. Johns, *J. Mol. Spectrosc.* **140** (1990) 353 ([https://doi.org/10.1016/0022-2852\(90\)90147-I](https://doi.org/10.1016/0022-2852(90)90147-I))
13. M. Niedenhoff, K. M. T. Yamada, S. P. Belov, G. Winnewisser, *J. Mol. Spectrosc.* **174** (1995) 151 (<https://doi.org/10.1006/jmsp.1995.1277>)
14. M. Niedenhoff, K. M. T. Yamada, G. Winnewisser, *J. Mol. Spectrosc.* **176** (1996) 342 (<https://doi.org/10.1006/jmsp.1996.0096>)
15. S. S. Brown, H. L. Berghout, F. F. Crim, *J. Chem. Phys.* **106** (1997) 5805 (<https://doi.org/10.1063/1.473246>)
16. S. S. Brown, H. L. Berghout, F. F. Crim, *J. Chem. Phys.* **107** (1997) 9764 (<https://doi.org/10.1063/1.475274>)
17. L. Fusina, I. M. Mills, *J. Mol. Spectrosc.* **86** (1981) 488 ([https://doi.org/10.1016/0022-2852\(81\)90296-4](https://doi.org/10.1016/0022-2852(81)90296-4))
18. M. Niedenhoff, K. M. T. Yamada, M. Winnewisser, S. C. Ross, *J. Mol. Struct.* **352–353** (1995) 423 ([https://doi.org/10.1016/0022-2860\(94\)08502-9](https://doi.org/10.1016/0022-2860(94)08502-9))
19. L. E. Snyder, D. Buhl, *Astrophys. J.* **177** (1972) 619 (<https://doi.org/10.1086/151739>)
20. A. Coutens, J. K. Jørgensen, M. H. D. van der Wiel, H. S. P. Müller, J. M. Lykke, P. Bjerkeli, T. L. Bourke, H. Calcutt, M. N. Drozdovskaya, C. Favre, E. C. Fayolle, R. T. Garrod, S. K. Jacobsen, N. F. W. Ligterink, K. I. Öberg, M. V. Persson, E. F. van Dishoeck, S. F. Wampfler, *Astron. Astrophys.* **590** (2016) L6 (<https://doi.org/10.1051/0004-6361/201628612>)
21. J. M. Jackson, J. T. Armstrong, A. H. Barrett, *Astrophys. J.* **280** (1984) 608 (<https://doi.org/10.1086/162033>)
22. N. Pinnavaia, M. J. Bramley, M.-D. Su, W. H. Green, N. C. Handy, *Mol. Phys.* **78** (1993) 319 (<https://doi.org/10.1080/00268979300100261>)
23. A. L. L. East, C. S. Johnson, W. D. Allen, *J. Chem. Phys.* **98** (1993) 1299 (<https://doi.org/10.1063/1.464298>)
24. M. Mladenović, *J. Chem. Phys.* **141** (2014) 224304 (<https://doi.org/10.1063/1.4903251>)
25. M. Mladenović, M. Lewerenz, *Chem. Phys.* **343** (2008) 129 (<https://doi.org/10.1016/j.chemphys.2007.06.033>)
26. M. Mladenović, M. Elhiyani, M. Lewerenz, *J. Chem. Phys.* **130** (2009) 154109 (<https://doi.org/10.1063/1.3111810>)
27. M. Mladenović, M. Elhiyani, M. Lewerenz, *J. Chem. Phys.* **131** (2009) 034302 (<https://doi.org/10.1063/1.3173275>)
28. *MOLPRO, a package of ab initio programs* (<http://www.molpro.net>)
29. M. Mladenović, P. Botschwina, C. Puzzarini, *J. Phys. Chem., A* **110** (2006) 5520 (<https://doi.org/10.1021/jp056743u>)
30. M. Mladenović, *J. Chem. Phys.* **112** (2000) 1070 (<https://doi.org/10.1063/1.480662>)

31. M. Mladenović, M. Lewerenz, *Chem. Phys. Lett.* **321** (2000) 135 ([https://doi.org/10.1016/S0009-2614\(00\)00321-3](https://doi.org/10.1016/S0009-2614(00)00321-3))
32. M. Mladenović, *Spectrochim. Acta, A* **58** (2002) 795 ([https://doi.org/10.1016/S1386-1425\(01\)00669-2](https://doi.org/10.1016/S1386-1425(01)00669-2))
33. V. E. Bondybey, J. H. English, C. W. Mathews, R. J. Contolini, *J. Mol. Spectrosc.* **92** (1982) 431 ([https://doi.org/10.1016/0022-2852\(82\)90113-8](https://doi.org/10.1016/0022-2852(82)90113-8))
34. J. H. Teles, G. Maier, B. A. Hess, Jr., L. J. Schaad, M. Winnewisser, B. P. Winnewisser, *Chem. Ber.* **122** (1989) 753 (<https://doi.org/10.1002/cber.19891220425>)
35. K. M. T. Yamada, *J. Mol. Spectrosc.* **81** (1980) 139 ([https://doi.org/10.1016/0022-2852\(80\)90334-3](https://doi.org/10.1016/0022-2852(80)90334-3))
36. M. Perić, M. Mladenović, S. D. Peyerimhof, R. J. Buenker, *Chem. Phys.* **86** (1984) 85 ([https://doi.org/10.1016/0301-0104\(84\)85158-7](https://doi.org/10.1016/0301-0104(84)85158-7)).